Astronomy & Astrophysics manuscript no. 3c295˙rev˙APH February 5, 2008
(DOI: will be inserted by hand later)

arXiv:astro-ph/0403401v1 17 Mar 2004

The faint X-ray Source Population near 3C 295

Valerio D'Elia[1], Fabrizio Fiore[1], Martin Elvis[2], Massimo Cappi[3], Smita Mathur[4], Pasquale Mazzotta[5], Emilio Falco[6], Filomena Cocchia[1]

[1] INAF-Osservatorio Astronomico di Roma
via Frascati 33, Monteporzio-Catone (RM), I00040 Italy.
[2] Harvard-Smithsonian Center for Astrophysics, Cambridge MA 02138, USA
[3] IASF-CNR, Bologna, Italy
[4] The Ohio State University, Columbus, OH 43210, USA.
[5] University of Durham South Road Durham DH1 3LE, UK
[6] Smithsonian Institution Whipple Observatory AZ 85645 USA

July 30 2003

Abstract. We present a statistical analysis of the *Chandra* observation of the source field around the 3C 295 galaxy cluster (z=0.46) aimed at the search for clustering of X-ray sources. We applied three different methods of analysis, all suggesting a strong clustering in the field on scales of a few arcmin. In particular 1) the logN-logS computed separately for the four ACIS-I chips reveals that there is a significant ($3.2\ \sigma$ in the $0.5-2$ keV, $3.3\ \sigma$ in the $2-10$ keV and $4.0\ \sigma$ in the $0.5-10$ keV band) excess of sources to the North-North East and a void to the South of the central cluster. 2) the two point, two-dimensional Kolmogorov-Smirnov (KS) test, shows the probability that the sources are uniformly distributed is only a few percent. 3) a strong spatial correlation emerges from the study of the angular correlation function of the field: the angular correlation function (ACF) shows a clear signal on scales of $0.5 \div 5$ arcmin, correlation angle in the $0.5-7$ keV band $\theta_0 = 8.5^{+6.5}_{-4.5}$, 90% confidence limit (assuming a power law ACF with slope $\gamma = 1.8$). This correlation angle is 2 times higher than that of a sample of 8 ACIS-I field at the $2.5\ \sigma$ confidence level. The above scales translate to $0.2 \div 2$ Mpc at the cluster redshift, higher than the typical cluster core radius, and more similar to the size of a "filament" of the large scale structure.

Key words. X-ray: background, X-ray: surveys, QSO: evolution

1. Introduction

N-body and hydrodynamical simulations show that clusters of galaxies lie at the nexus of several filaments of galaxies (see e.g. Peacock 1999, Davè et al. 2001 and references therein). Such filaments map out the "cosmic web" of voids and filaments of the large scale structure (LSS) of the Universe. According to the same simulations these filaments contain a large fraction ($30-40\%$) of the baryons in the Universe at z<1 (the remainder ending up in the hot gas in clusters of galaxies on one side, and in stars and cold gas clouds on the other side). Despite its larger total mass, observations of the intergalactic matter in filaments have yielded so far only limited information, mostly due to its low density (most of the baryons in this phase should be at densities only 10-100 times higher than the average density in the Universe). The most direct ways to detect a filament at low redshift is through its soft X-ray diffuse emission (see e.g. Zappacosta et al. 2002, Soltan, Freyberg & Hasinger 2002), or through soft X-ray and UV absorption line studies (see e.g. Fiore et al. 2000 and references therein, Nicastro et al. 2002, Nicastro et al. 2003, Mathur et al. 2003). Both methods require very difficult observations, at the limit of the present generation of X-ray and UV facilities. Alternatively, filaments could be mapped out by galaxies (Daddi et al. 2001, Giavalisco & Dickinson 2001) and by the much more luminous Active Galactic Nuclei (AGNs), assuming that AGNs trace galaxies. Since rich clusters of galaxies are good indicators of regions of sky where filaments converge, numerous AGN searches around clusters of galaxies have been performed in the past. Several of these studies suggest overdensities of AGNs around distant clusters of galaxies (Molnar et al. 2002 for the cluster Abell 1995; Best et al. 2002 for MS1054-03; Martini et al. 2002 for Abell 2104; Pentericci et al. 2002 for the protocluster at $z \sim 2.16$ around the radio galaxy MRC 1138-206; see also Almaini et al. 2003 for the ELAIS North field). Many of these studies have been performed in X-rays, since extragalactic X-ray sources, which are mostly AGNs, have a space density ~ 10 times higher than optically selected AGNs (see Yang et al. 2003),

and therefore provide denser tracing of LSS. One of the first studies of the X-ray source population in cluster fields was performed by Cappi et al. (2001) who studied the *Chandra* 8×8 arcmin ACIS fields around the distant cluster of galaxies RX J003033.2+261819 ($z = 0.5$) and 3C 295 ($z = 0.46$). Cappi et al. (2001) reported the tentative detection of an overdensity of faint X-ray sources in a region of a few arcmin around both clusters, with respect to the average X-ray source density at the same flux limit. However, the observations were too short ($\sim$ 30 ks and $\sim$ 18 ks, respectively), and the source samples consequently too small, to derive any more detailed conclusion.

In addition to counting sources in selected sky areas, the clustering of X-ray sources can be studied using other observational and statistical tools. Gilli et al. (2003) report narrow spikes in the redshift distribution of the sources in the *Chandra* Deep Field South (CDFS), indicating strong clustering of sources in these narrow redshift ranges. If the source samples are sufficiently large (of the order of 100 sources or more) one derives more detailed and quantitative information on the source clustering by studying the angular correlation function (ACF) of the sources in the field. Vikhlinin & Forman (1995) were among the first to study the ACF in the X-ray band; they evaluated an average ACF from a large set of deep ROSAT observations, covering in total 40 deg^2 of sky. They found positive correlation on scales from a fraction of arcmin to tens of arcmin. However, their best fit "correlation angle" $\theta_0 \sim 10$ arcsec, is smaller than the ROSAT PSPC Point Spread Function ($\sim$ 25 arcsec FWHM on-axis); as noted by the authors, this leads to an "amplification bias" and their measured ACF is consequently somewhat overestimated.

This effect can be greatly mitigated by using a telescope like *Chandra*, whose on-axis PSF is only 0.5 arcsec FWHM, 50 times better than the PSPC on-axis PSF. So far a correlation analysis of *Chandra* X-ray sources have been published only by Giacconi et al. (2000), who used the first 100 ks of observation of the CDFS, and by Yang et al. (2003) who analyzed a mosaic of 9 moderately deep (30ks) *Chandra* pointings of the Lockman Hole area. Yang et al. could study the source angular correlation on scales of several tens of arcmin, being limited on smaller scales by the small number of detected sources per unit area.

Our main goal in this paper is to push this kind of analysis toward a) smaller scales, of order of a few arcmin; and b) targeting a field where the likelihood of observing LSS is high, i.e. a field around a cluster of galaxies. For these reasons we observed again with *Chandra* for about 100ks the 3C295 field, where Cappi et al. (2001) found tentative evidence of an overdensity of faint X-ray sources in a region of a few arcmin around the central cluster.

The paper is organized as follows: Section 2 presents the observations and data reduction; Section 3 presents the results of our analysis; Section 4 discusses such results and draws our conclusions.

2. *Chandra* observations and data reduction

Chandra observed the $16' \times 16'$ field around the 3C 295 cluster with ACIS-I (Garmire 1997) on 2001, May 18. The aim point of the observation is located at the position of 3C 295 $\alpha = 14{:}11{:}10$, $\delta = +52{:}13{:}01$ (J2000) and exposure time is $\sim$ 92 ks. The data reduction was carried out using the *Chandra* Interactive Analysis of Observations (CIAO) software version 2.1.3 (http://cxc.harvard.edu/ciao). No strong background flares are present in the observation. All the data analysis has been performed separately in the soft $0.5-2$ keV band, in the hard $2-7$ keV band and in the broad $0.5-7$ keV band. Since the ACIS background rises sharply above $\sim$ 7 keV, we excluded all data with $E > 7$ keV.

In order to check our analysis method, an identical analysis was performed for the *Chandra* Deep Field South (CDFS, see Giacconi et al. 2002) in the $0.5-2$ keV and $2-7$ keV bands. The CDFS is a collection of 11 separate ACIS-I observations centered on the same point, α =03:32:28.0, $\delta = -27{:}48{:}30$ (J2000), but with different roll angles. For this reason, the effective exposure time changes in different regions of the field. For the CDFS analysis we selected only the region with the maximal effective exposure time, which is $\sim$ 942 ks; a region that is slightly smaller than the full 3C 295 field.

In the following subsection the source detection procedure is described, while subsection 2.2. deals with the sky coverage evaluation, which will be used in section 3 for the logN-logS calculation.

2.1. Source detections

The source detection was carried out using the 'PWDetect' algorithm. This is a wavelet-based source detection code for *Chandra* X-ray data developed at the Osservatorio Astronomico di Palermo (Damiani et al. 1997a, 1997b). PWDetect performs a multiscale analysis of the data, allowing detection of both pointlike and moderately extended sources in the entire field of view. This detection algorithm was compared with other detection tools, namely, the CIAO detection tool CELLDETECT and the Ximage DETECT. The latter algorithms detected a smaller number of sources than PWDetect in both the CDFS and 3C 295 field, and in all energy bands. In addition, they tended to find extended sources as multiple detections.

PWDetect requires a *Chandra* FITS event file and the associated exposure map as inputs. The exposure maps were computed using the CIAO task MKEXPMAP for each ACIS-I chip and then combined together into the single exposure map required by PWDetect for each of the $0.5-2$ keV, $2-7$ keV and $0.5-7$ keV energy bands. The sources were detected using minimum and maximum wavelet scales of 0.5 and 16 arcsec, respectively. We assumed a probability detection threshold of 2×10^{-5}. Since the local background level is of the order of 0.1 cts/arcsec^2, the minimum number of counts for a source

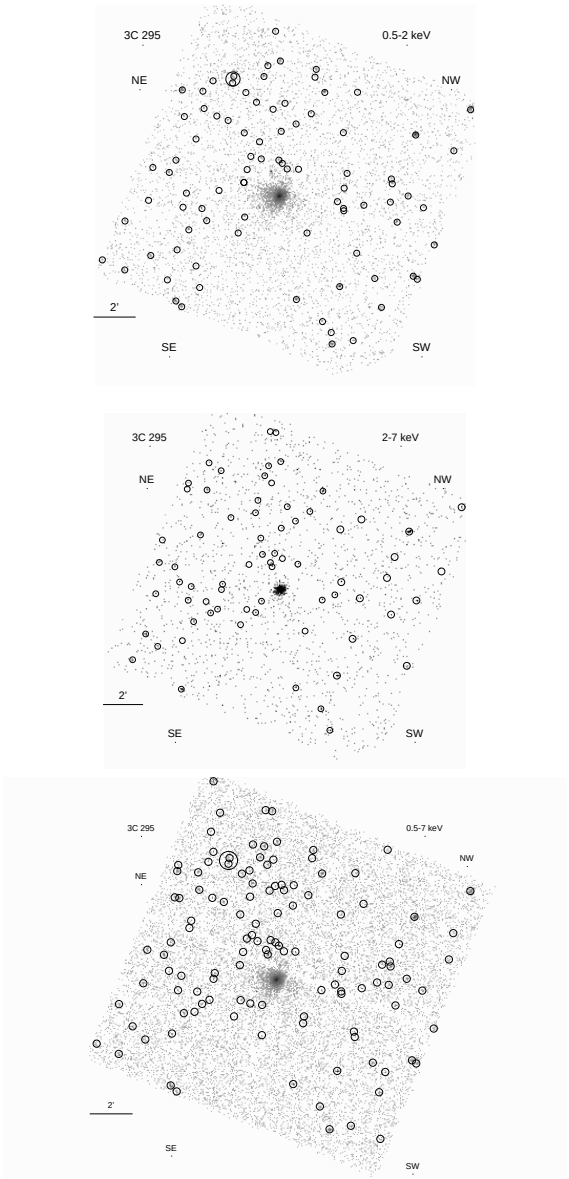

Fig. 1. The *Chandra* 3C 295 field in the $0.5-2$ keV band (upper panel), in the $2-7$ keV band (central panel) and in the $0.5-7$ keV band (bottom panel). Circles represent the sources detected with the wavelet-based source detection code 'PWdetect'. The largest circles in the upper and bottom panels indicates a very extended source, possibly a group of galaxies. The brightest source in the center of the field is the cluster of galaxies 3C 295.

to be detected is ~ 7. The assumed probability and the number of independent cells used by PWdetect give the expected number of spurios sources per field; this number results to be < 1 in all energy bands. We identified 89 sources in the $0.5-2$ keV band lying within the flux range $3.2\times10^{-16}-4.4\times10^{-13}$ ergs cm^{-2} s^{-1}, 71 sources in the $2-7$ keV band within the flux range $1.7\times10^{-15}-5.8\times10^{-14}$ ergs cm^{-2} s^{-1} and 121 sources in the $0.5-7$ keV band in the flux range $8.8\times10^{-16}-1.2\times10^{-13}$ ergs cm^{-2} s^{-1}. The central cluster was not considered in the analysis, thus we excluded the detections in the $\sim 2'\times2'$ central region. The counts in the $0.5-2$ keV, $2-7$ keV and $0.5-7$ keV bands were converted in $0.5-2$ keV, $2-10$ keV and $0.5-10$ keV fluxes, respectively, by multipling the counts by the conversion factors 5.65×10^{-12}, 2.70×10^{-11} and 1.24×10^{-11} (from PIMMS: http://heasarc.gsfc.nasa.gov/Tools/w3pimms.html). These factors are appropriate for a $\Gamma = 1.8$ power law spectrum with a Galactic absorption toward the 3C 295 field of $N_H = 1.33\times10^{20}$ cm^{-2} (Dickey & Lockman 1990), and take into account the quantum efficiency degradation of the ACIS chips (http://asc.harvard.edu/cal/Acis).

Fig. 1 shows the 3C 295 field in the first two bands; the detected sources are indicated by circles. The larger circle in the upper left chip of the $0.5-2$ keV picture indicates an extended source (detected on a 16 arcsec scale, see next subsection) which is probably a group or a cluster of galaxies. A close observation of this region shows other count peaks which could be other X-ray sources, possibly the galaxies in the group, below the detection threshold, althouh they may be spurious detections caused by positive fluctuations of the surface brightness.

Visually the sources give a strong impression of being concentrated to the East, and expecially the NE. This is the same trend reported in Cappi et al. (2001). We will proceed to quantify this impression in the following sections.

2.2. Extended sources

As mentioned before, in the soft and broad band, we identified an extended source on a scale of 16 arcsec, which could also be two or more confused point sources. This source is marked in fig. 1 by a large circle and its position is ra = 14 : 11 : 37, dec = +52 : 18 : 35; its $0.5-2$ keV flux is 4.4×10^{-15} ergs cm^{-2} s^{-1} and the $0.5-7$ keV one is $= 1.1\times10^{-14}$ ergs cm^{-2} s^{-1}. In fig. 2 we show the contours of the $0.5-7$ keV image superimposed to the image taken at the TNG with the DOLORES camera on march 19, 2002, with an exposure time of 900 s; the seeing was 1.3 arcsec and the limiting magnitude $R_{lim} = 24.1$. The southern strong X-ray emitter, which is a pointlike source, has no optical counterpart down to the limiting magnitude of the observation, while the extended emission is centered on two bright $R_{mag} \sim 18.5$ galaxies. Tab. 1 reports the magnitudes of the galaxies marked with capital letters in Fig. 2.

If we assume that these galaxies are at a z similar to that of 3C 295, $z = 0.46$, then their absolute magnitude is $M_B \simeq -23$. This is almost two orders of magnitude more luminous than the break magnitude of the galaxy luminosity function at $z = 0.5$, that is $M_B^* = -21.3$ (e.g. Poli et al. 2003). Moreover, we note that the central radio galaxy of the 3C 295 cluster has $R_{mag} = 18.4$ in our image, while the X-ray flux of the 3C 295 cluster is $\sim 1.0\times10^{-12}$ ergs cm^{-2} s^{-1} in the $0.5-4.5$ keV (see e.g. Henry & Henriksen). We conclude that it is unlikely that the optical sources

Table 1. Observed optical magnitudes in the R band of the sources in fig. 2

sources	R_{mag}
A	18.8
B	18.15
C	19.11
D	17.95
E	18.18
F	19.11

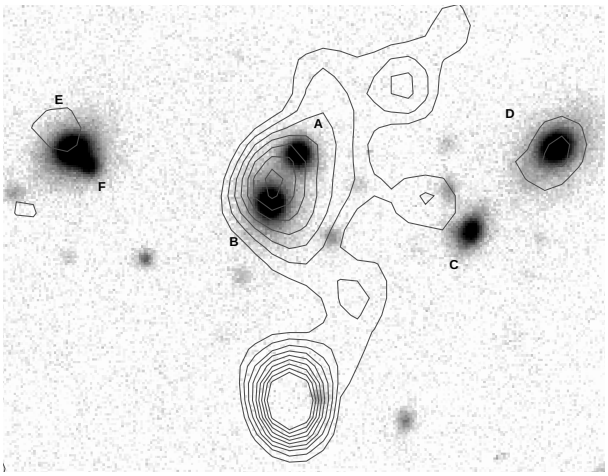

Fig. 2. The contours of the 0.5−7 keV band image overimposed to the optical (R band) image of the extended source identified in the soft and broad band. Capital letters are associated to galaxies whose R observed magnitudes are reported in tab. 1.The image width is ~ 1.25 arcmin

corresponding to the extended x-ray emission are located at $z = 0.46$. Since the extended source is not detected in the $2 - 7$ keV band, we can only put an upper limit on the temperature of the putative cluster or group; using a Raymond-Smith model with solar abundances ratio of 0.4, we find $T < 3$ keV if we assume the same redshift of 3C 295 and $T < 2$ keV for $z = 0$. On the other hand, an upper temperature of $2 \div 3$ keV poses an upper limit on the luminosity and thus on the redshift; unfortunately, this limit is not significant for our purposes.

We checked for other signs of diffuse emission in the 3C 295 field, and in particular in the NE region, where the detected sources appear to be concentrated. To do this, we subtracted the detected sources from the image and we computed the average background level of the observation in the $0.5 - 7$ keV band; the central part of the image was excluded because of the high level of counts due to the central cluster. Next, we compared this background level with the counts evaluated in 25 regions of the field. The area of the regions has been chosen to vary in the range $10^3 \div 10^4$ arcsec^2. The excess with respect to the background, if any, is never significant at $> 3\ \sigma$ confidence level. Counts were converted to fluxes assuming a Raymond-Smith model with $T = 1$ keV, and a solar abundances ratio of 0.4. The $3\ \sigma$ upper limit on the flux is then 2.7×10^{-14} ergs cm^{-2} s^{-1} arcmin^{-2}. Thus we can conclude that any diffuse emission is too faint to be detected.

2.3. Sky coverage

'Sky coverage' defines the area of the sky sensitive to a given flux limit, as a function of flux. Due to vignetting effects and to the increase of the size of the PSF in the outer regions of the detector, the center of the ACIS-I field of view is the most sensitive: i.e. for a given exposure time, the central part of the detector is able to detect fainter sources than the outer regions. Thus, one must take into account this effect while computing the logN-logS, that is, the number of sources whose flux exceeds a given flux limit.

As a preliminary step to evaluating the sky coverage, we computed background maps for the two energy bands using the Ximage package. We did this by subtracting the central part of the field (the same $\sim 2' \times 2'$ region centered on the 3C 295 cluster excluded from the source detection) and excluding all the sources detected in the images. In order to calculate the sky coverage, these maps and the exposure maps were rebinned into 128×128 matrices of ~ 10 arcsecs per pixel.

We also studied the increasing apparent size of the detected sources with the off-axis angle (i.e., the distance of the source from the aim point); both quantities are supplied by the detection algorithm. We used the rebinned background maps to calculate the background for all the points in the field in different size regions according to the relation between apparent size and off-axis. The local background level was used to calculate the minimum number of counts needed to exceed the noise in the case of Poisson statistics, to exceed the probability threshold of 2×10^{-5}. This value assures a number of spurious sources per field < 1 in all energy bands (see previous subsection). The minimum counts were divided by the exposure map and thus converted to minimum detectable fluxes. The sky coverage at a given flux f is simply the sum of all the regions of the detector whose minimum detectable flux is lower than f, and can be easily converted into deg^2. The sky coverage computed with such a method for the three energy bands is shown in fig. 3.

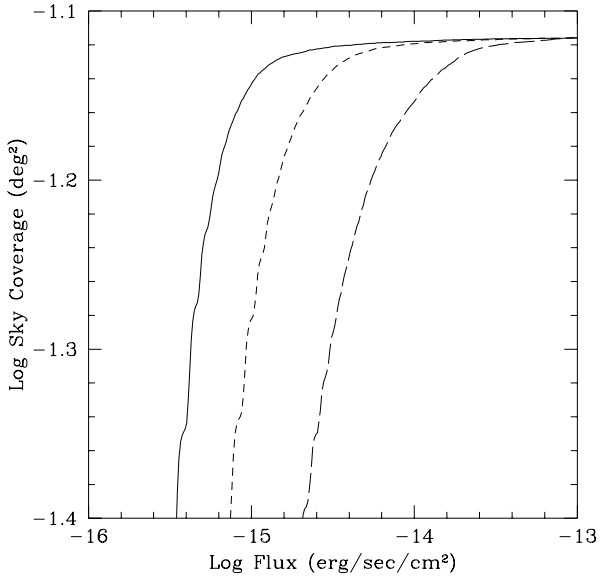

Fig. 3. The sky coverage (area covered vs. flux limit) for the $0.5-2$ keV band (solid line), for $2-10$ keV band (long dashed line) and for the $0.5-10$ keV band (short dashed line).

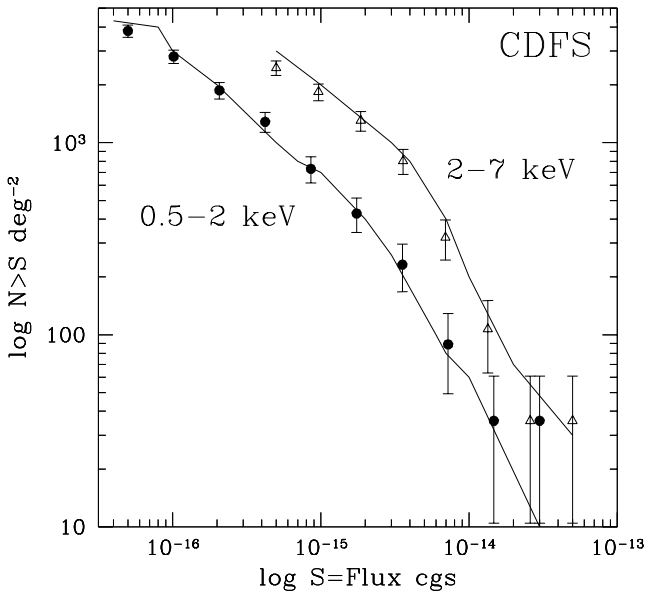

Fig. 4. The *Chandra* Deep Field South logN-logS in the $0.5-2$ keV band (filled circles) and in the $2-10$ keV band (open triangles) evaluated in this paper. Errors represent 1σ confidence limit. Solid lines represent the CDFS LogN-LogS from Rosati et al. (2002).

3. Results

3.1. logN-logS

3.1.1. Checking the analysis method

To check the validity of our analysis method, we computed the LogN-LogS of the CDFS and we compared this with previous computations (Rosati et al. 2002); the agreement is quite good (see fig. 4). Then we computed the logN-logS for 3C 295 in the three energy bands weighting the number of sources at a given flux with the sky coverage at the same flux; in fig. 5 is shown the LogN-LogS for the $0.5-2$ and $2-7$ keV band. The CDFS logN-logS extends to lower fluxes than the 3C 295 one, because the exposure time is about 10 times longer, and the error are similar in the region of flux overlap for the two field. There is excellent agreement between the number counts for the two fields.

3.1.2. Chip-by-chip LogN-LogS

While the average 3C 295 logN-logS appears normal, our goal is to search for inhomogenities within the ACIS-I field. The most natural way to do it is to derive the logN-logS for each $8'\times8'$ ACIS-I chip, separately. The logN-logS for each ACIS-I chip, in each of the three bands, is shown in Fig. 6. The logN-logS in the upper left quadrant is significantly higher than that of the lower right chip, up to 2×10^{-15} ergs cm^{-2} s^{-1} in the $0.5-2$ keV band, up to 6×10^{-15} ergs cm^{-2} s^{-1} in the $2-10$ keV band, and up to 10^{-14} ergs cm^{-2} s^{-1} in the $0.5-10$ keV one.

To be more quantitative, we fitted a power law to the four ACIS-I logN-logS in each band, in the $3\times10^{-16}-2\times10^{-14}$ ergs cm^{-2} s^{-1} flux range for the soft band, $3\times10^{-15}-2\times10^{-14}$ ergs cm^{-2} s^{-1} for the hard band, and $6\times10^{-16}-2\times10^{-14}$ ergs cm^{-2} s^{-1} for the $0.5-10$ keV band. Table 1 shows the results of the LogN-LogS fits for the two fields. In Fig. 7 we plot the slope of the LogN-LogS power law versus the normalization at 5×10^{-16} ergs cm^{-2} s^{-1} for the soft band, at 5×10^{-15} ergs cm^{-2} s^{-1} for the hard band and at 10^{-15} ergs cm^{-2} s^{-1} for the total band; error bars represent the 90% confidence limit. Though the slopes of the four logN-logS are all compatible within the errors, the normalization of the NE LogN-LogS chip is clearly higher than that of the three other chips for all three bands. The best fit for the CDFS is shown with dashed lines and appear to be consistent with the latter chips, both for slope and normalization. To give some numbers, the NE chip differs in normalization from the SW one by 3.2 σ in the soft band, by 3.3 σ in the hard one and by 4.0 σ in the total band. We note that in the total band, the significance of the discrepancy between the NE and SE chip is higher. This is due to the higher statistics that can be achieved using the whole energy range of the observation.

In the next subsections we will study in more detail the distribution of the sources, in particular how much it differs from the uniform distribution, and its angular correlation function.

3.2. Two-dimensional Kolmogorov-Smirnov test

In this subsection we apply a two-dimensional Kolmogorov-Smirnov (KS) test to check whether

Table 2. Results of the four 3C 295 chips and CDFS LogN-LogS fit

	$0.5-2$ keV			$2-10$ keV			$0.5-10$ keV		
	sources	slope	normaliz.	sources	slope	normaliz.	sources	slope	normaliz.
3C 295	89	$-0.75^{+0.09}_{-0.1}$	1000^{+100}_{-100}	71	$-1.3^{+0.2}_{-0.2}$	390^{+60}_{-50}	121	$-0.9^{+0.1}_{-0.2}$	1300^{+200}_{-200}
NE	36	$-0.8^{+0.1}_{-0.2}$	1600^{+600}_{-400}	29	$-1.6^{+0.4}_{-0.6}$	900^{+300}_{-300}	53	$-0.7^{+0.1}_{-0.1}$	2600^{+600}_{-600}
NW	18	$-0.7^{+0.2}_{-0.3}$	700^{+300}_{-400}	13	$-1.4^{+0.7}_{-0.9}$	300^{+200}_{-100}	23	$-0.7^{+0.2}_{-0.2}$	1000^{+300}_{-300}
SW	12	$-0.7^{+0.2}_{-0.3}$	600^{+300}_{-300}	7	$-1.1^{+0.7}_{-1.0}$	200^{+200}_{-100}	17	$-0.6^{+0.2}_{-0.2}$	700^{+400}_{-300}
SE	23	$-1.0^{+0.3}_{-0.4}$	950^{+400}_{-300}	22	$-1.6^{+0.7}_{-0.9}$	500^{+200}_{-200}	28	$-0.8^{+0.1}_{-0.2}$	1300^{+500}_{-300}
CDFS	202	$-0.9^{+0.1}_{-0.1}$	900^{+100}_{-100}	151	$-1.7^{+0.2}_{-0.2}$	280^{+40}_{-40}	-	-	-

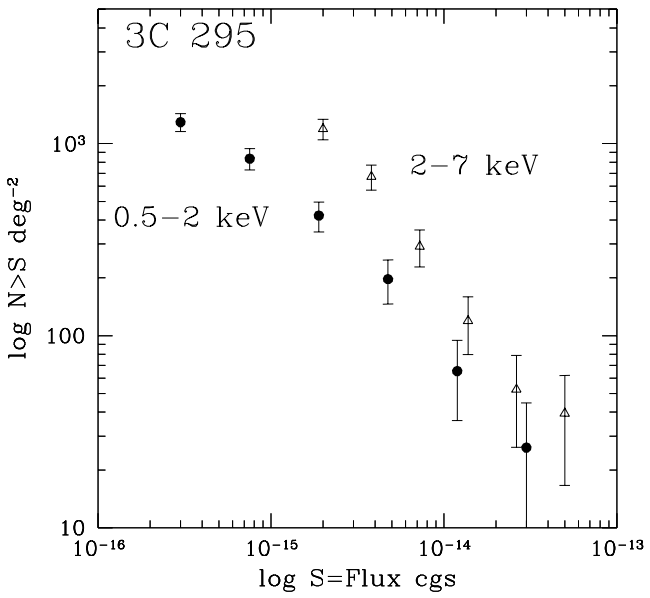

Fig. 5. The 3C 295 logN-logS in the $0.5-2$ keV band (filled circles) and in the $2-10$ keV band (open triangles) evaluated in this paper. Errors represent 1σ confidence limit.

the distribution of the sources is uniform or not. The 1-D KS test is a simple and powerful tool to test whether two data sets are drawn from the same distribution, or whether a data set is compatible with a given distribution, provided that these data sets and distributions are functions of only one variable. The KS test makes use of the parameter D, which represents the maximum value of the absolute difference between the cumulative distributions drawn from the two data sets, or from the data set and the given distribution. Once D is known, the probability that a larger value of D can be observed if the two distributions are identical is given by:

$$P(D > observed) = 2\sum_{i=1}^{\infty}(-1)^{i-1}e^{-2\,i^2\,\lambda^2}, \qquad (1)$$

where λ is a simple function of D.

The generalization of the KS test to a two-dimensional distribution is due to Peacock (1983) and Fasano & Franceschini (1987). Any point of a data set is now defined by a pair of coordinates, which in turn define a plane. Thus, given a point of the data set, one can compute how many elements (of the same data set or of another one) occupy the four quadrants defined by such a point, or how many points are expected in the four quadrants according to the given distribution. The parameter D can now be defined as the maximum value of the absolute difference between the number of elements of the two data set (or of the data set and the distribution) in the quadrants, as the reference point changes within the data set. Fasano & Franceschini (1987) demonstrated that eq. (1) holds even for two-dimensional distributions, provided that

$$\lambda = \frac{\sqrt{N}\,D}{1+\sqrt{1-r^2}\,(0.25-0.75/\sqrt{N})}; \qquad (2)$$

here N is the number of elements of the data set (or $N = N_1\,N_2/(N_1+N_2)$ if two data sets are involved) and r is the correlation coefficient of the two variables of the data set (or the average between the two correlation coefficients in the two data set case).

We have used eq. (1) and (2) to test the hypothesis that the distribution of the sources in the 3C 295 field is uniform. Since the sources are not uniformly distributed due to the sensitivity of the instrument being higher in the middle of the detector (see section 2.2), thus low flux sources can only be found near the centre of the four ACIS-I chips, so we imposed a higher minimum flux. We specified this minimum flux as the one which could have been detected at least in 75% of the detector area. We note that this effect is not very strong in the 3C 295 field, because the central part of the detector was excluded due to the presence of the cluster. We found the probability that the distribution of the 3C 295 sources is uniform is very low: $\sim 3\%$, $\sim 4\%$ and $\sim 0.6\%$ in the $0.5-2$, $2-7$ and $0.5-7$ keV bands, respectively (see also table 2).

3.3. Angular correlation function

Although the LogN-LogS and the 2-D KS test show that the sources in the 3C 295 field are not uniformily distributed, they do not give angular information on the spatial distribution of the sources. The conventional way to determine the spatial correlation of sources in a field is to use the 'two point angular correlation function' (ACF, Peebles 1980, Peacock 1999). This function measures the

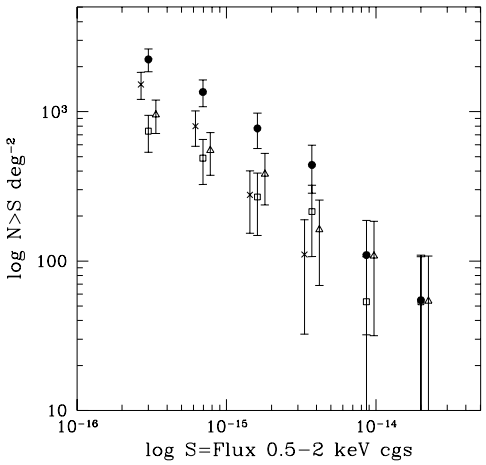

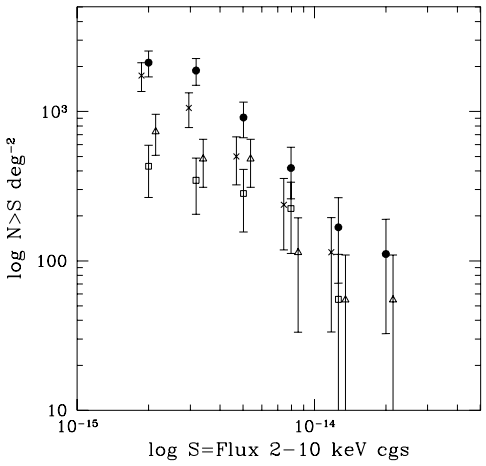

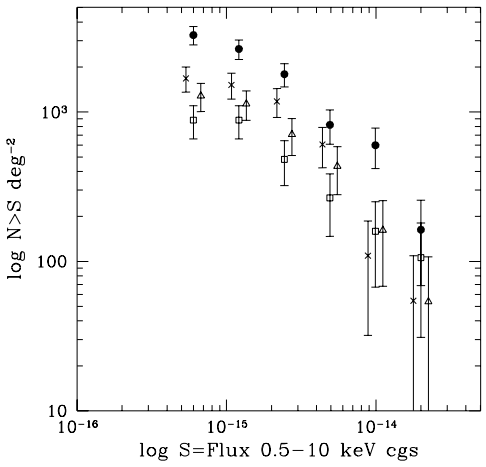

Fig. 6. The mean (whole field) 3C 295 logN-logS in the $0.5-2$ keV band (upper panel), in the $2-10$ KeV band (central panel) and in the $0.5-10$ keV band (lower panel), calculated for each ACIS-I chip separately. Filled circles represent counts for the NE chip, open triangles for the NW, open squares for the SW and crosses for the SE. For clarity reasons, the points for SE chip and the NW have been shifted slightly to the left and to the right, respectively. Errors represent 1σ confidence limit.

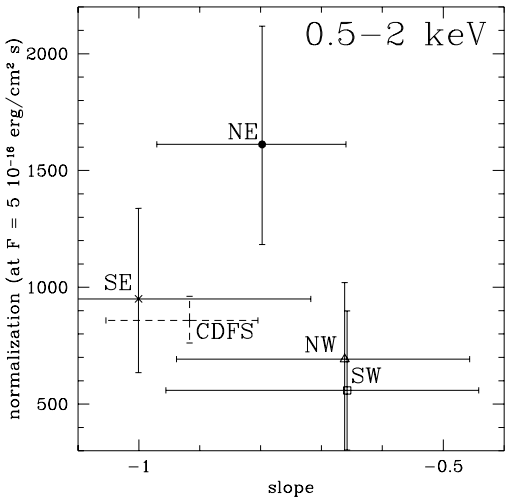

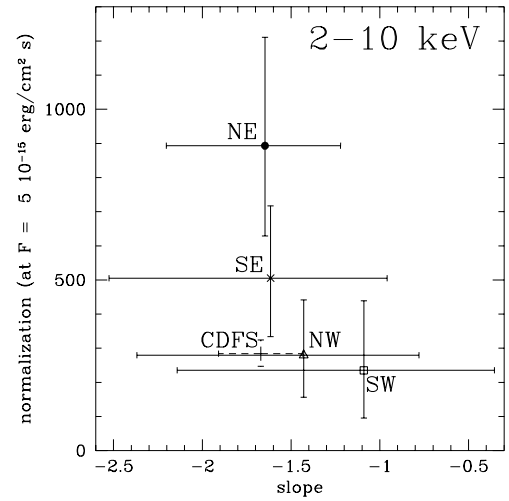

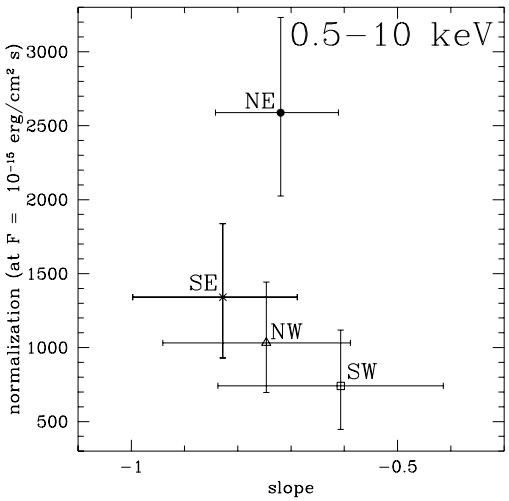

Fig. 7. Results of the power law fits to the four logN-logS chips in the soft band (upper panel), in the hard band (central panel) and for the whole band (lower panel). x axis plots the slope of the power law, while on the y axis is plotted the normalization at 5×10^{-16} ergs cm^{-2} s^{-1} (soft band), at 5×10^{-15} ergs cm^{-2} s^{-1} (hard band) and at 10^{-16} ergs cm^{-2} s^{-1} (whole band). Filled circles represent the NE chip, open triangles the NW, open squares the SW and crosses the SE. Dashed lines represent the fit for the CDFS. Errors are the 90% confidence limit.

strength of the spatial correlation, but does not say anything about where the sources are clustered. This function is given by the following relation:

$$w(\theta) = \frac{DD}{RR} - 1, \qquad (3)$$

where DD is the ratio of pairs of sources in the real data, which fall in the separation angle $(\theta,\, \theta + d\theta)$ and the RR is the number of those pairs expected when the spatial distribution of sources is random. To compute the ACFs, we proceeded as follows: we computed the angular separation for the pairs in our data set; we generated a random uniform distribution of 1000 sources in the same area and we computed their angular separation; we evaluated the ACFs using eq. (3) and rescaling RR to the number of pairs of the real field. We made the same flux cut-off to take into account the higher sensitivity of the detector in its central region (see previous subsection). Fig. 8 shows the ACFs for the 3C 295 field.

The errors in fig. 8 were estimated using two different methods. The first one (solid lines) is simply the Poisson statistics, the error is defined as the inverse of the square root of the real pair number (Peebles 1980) and is show in fig. 8 with solid lines. The second one (dashed lines) is more accurate and is called the bootstrap resampling method (see Barrow, Bhavsar & Sonoda 1984 and references therein). Briefly, we generated 100 simulated fields from the real one, by randomly selecting within the sources of the field a number of sources equal to the data set size. This produces simulated fields with a number of elements equal to that of the real field, but with some sources counted more than once and others not considered at all. The bootstrap method consists in recalculating the ACF using such simulated fields and in calculating the error as the standard deviation of the 100 ACFs obtained in this way. The bootstrap errors (which probably overestimate the true error) exceed the Poisson ones. This is because the Poisson errors depend on the number of pairs at each scale, while the bootstrap ones also depend on how many pairs are produced by each single source. In more detail, let us suppose that a large number of sources are distributed along a circumference, and one is placed at its centre; obviously, a strong angular correlation will be found at scales equal to the circle's radius. Poisson errors will be strongly reduced as the number of sources along the circumference increases, ignoring that a single source (namely, the central one) strongly boosts the correlation; bootstrap errors take this effect inThe other way roundto account by randomly excluding or counting more than once the central source, when recomputing the ACF.

Fig. 8 (long dashed line) also shows the best fit for the angular correlation function found by Vikhlinin & Forman (1995) for an extensive set of deep ROSAT observations covering 40 deg^2 of sky. Their power law model $w(\theta) = (\theta/\theta_0)^{(1-\gamma)}$ yields the best fit parameters $\theta_0 = 10 \pm 8$ arcsecs and $\gamma = 1.7 \pm 0.3$. However they found that the correlation angle θ_0 was smaller than the FWHM of the ROSAT PSPC PSF, which is ~ 25 arcsec on-axis, which

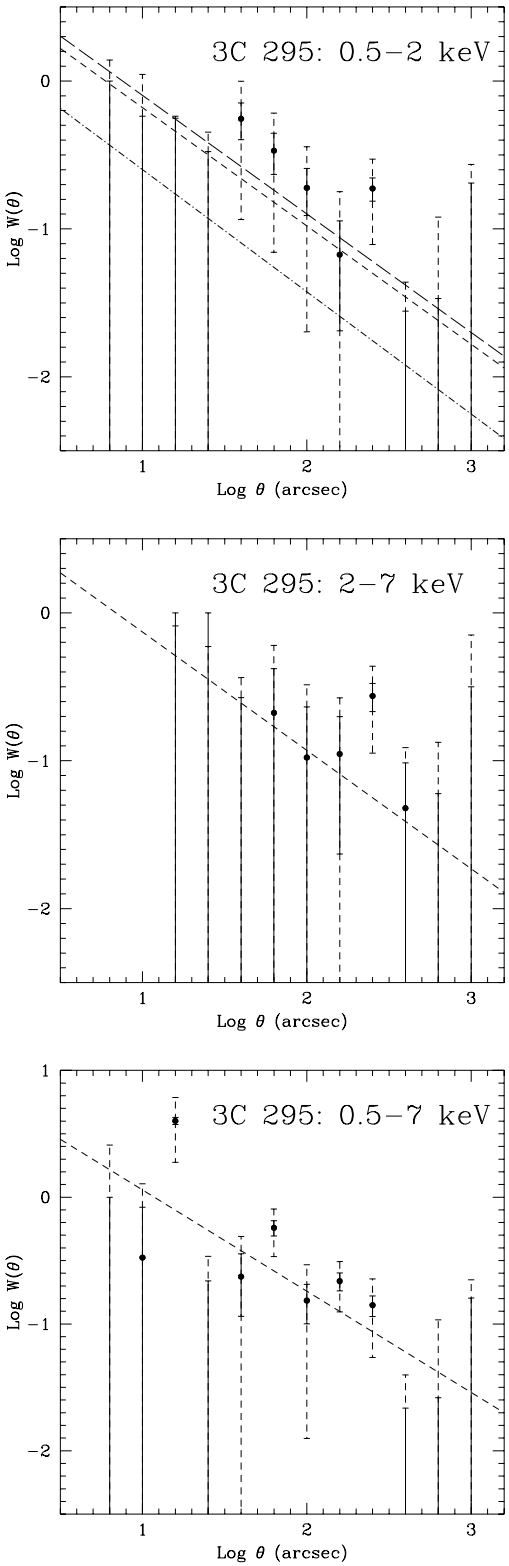

Fig. 8. The 3C 295 angular correlation function in the $0.5 - 2$ keV band (upper panel), in the $2 - 7$ keV (central panel) and in the $0.5 - 7$ keV band (lower panel). Solid error bars are Poisson; dashed error bars are bootstrap. Short-dashed lines represent our fit to the data assuming bootstrap error bars. The long dashed line represents the best fit found by Vikhlinin & Forman (1995) for ROSAT sources; the dot-dashed line is the simulated ACF calculated by the same authors in order to correct the effect of the amplification bias.

leads to an amplification bias. Simulations to correct for this gave the ACF show in Fig. 8 with a dot-dashed line, which has a normalization 2.85 times smaller (Vikhlinin & Forman 1995). This means that the uncorrected Vikhlinin & Forman (1995) ACF (long dashed line) represents a strong upper limit to the ROSAT ACF. Since the ROSAT PSPC energy band is 0.1-2 keV we cannot compare the VK85 ACF with our ACFs in the hard (2 - 7 keV) and whole (0.5 - 7 keV) bands.

Vikhlinin & Forman (1995) sample could only produce the ACF down to a ~ 30 arcsec scale ($Log\theta = 1.5$).

For the 3C 295 field in the $0.5-2$ keV band, we found a signal above the upper limit of the Vikhlinin & Forman (1995) fit on scales $\sim 60 - 240$ arcsec, if we use the Poissonian error bars; however using the bootstrap errors reduces this scale to only ~ 240 arcsec. A similar effect is present in the $2-7$ keV band, where a clear signal of correlation emerges on scales of ~ 240 arcsec assuming both Poisson and bootstrap statistics. A stronger and wider signal is present in the $0.5-7$ keV band, on scales ranging from ~ 15 arcsec to ~ 240 arcsec. This reflects the clustering of the sources clearly visible in the upper left corner of fig. 1 (on linear scales of the order of half a chip length, ~ 240 arcsec). The improved statistics in the $0.5-7$ keV band, due to the higher number of sources detected, gives rise to a stronger signal.

The short-dashed lines in fig. 8 represent the fit of $w(\theta) = (\theta/\theta_0)^{1-\gamma}$ to our data, assuming the bootstrap error bars; $\gamma = 1.8$ was fixed as in Vikhlinin & Forman (1995). In the soft band we found $\theta_0 = 6.0^{+4.4}_{-3.7}$ arcsec, in the hard band $\theta_0 = 6.9^{+6.9}_{-5.1}$ arcsec, and in the broad band $\theta_0 = 8.5^{+6.5}_{-4.5}$ arcsec (90% confidence limit). These values are consistent within their relatively large error to the Vikhlinin & Forman (1995) fit for θ_0 without correcting for the amplification bias ($\theta_0 \sim 10$ arcsec). If we assume the Poisson error bars, the value of θ_0 rises and the errors become smaller in all energy bands.

Finally, we checked the dependance of the ACF on the flux limit. We computed the ACF in the broad band for three different flux limits (i.e., 1 times, 2 times and 3 times the flux limit given in tab. 2, footnote *a*) and we found that θ_0 vary less than 25%, while its error increases with the flux limit.

3.3.1. CDFS

We applied the KS test and evaluated the ACF for the CDFS in order to check whether this field is different from 3C 295.

Table 2 shows the results of the two dimensional KS test. We can see that CDFS is compatible with a uniform distribution with a higher probability ($\sim 15\%$) than 3c 295 ($\sim$ a few %). We note that the KS test result depends on the minimum flux chosen; nevertheless, KS for CDFS gives a higher probability of a uniform distribution than 3C295 even if we use for the two observations the same flux limit. The first and the third column of table 2 report the KS results for the flux limit described in this subsection; the second column shows the CDFS results for a flux limit equal to that of 3C 295.

In fig. 9 we show the ACF for the CDFS field; in both the energy bands we found no evidence of a strong signal such as that featured by the 3C 295 field. Giacconi et al. (2001) evaluated the CDFS ACF for the first 100 ks observation of the CDFS; so, we checked our algorithm by calculating the ACF for the same data and found, reassuringly, agreement within 1 σ.

3.3.2. ACF in 8 selected *Chandra* Fields

In order to check whether or not the strong clustering of the 3C 295 field is peculiar, the comparison with the CDFS is not enough, and a larger sample of *Chandra* ACIS-I fields of similar exposure time has to be analyzed. For this reason, we browsed the *Chandra* data archive and matched all the ACIS-I observations belonging to the classes "AGNs" and "Surveys", with an exposure time of at least 50 ks. We used the detection algorithm PWDetect on these fields to detect sources in the three energy bands. In tab. 4 we show the 8 fields selected for this analysis, their exposure times and the sources detected in the three bands.

We computed the ACF in the $0.5-7$ keV band using a flux cut-off such that the minimum flux could have been detected at least in 75% of the detector area, as we did for 3C 295. The average ACF of this sample is shown in fig. 10. Though a signal is still present at scales > 100 arcsec, it is clearly weaker than that of 3C 295. To be more quantitative, we fitted these data with a power law of fixed slope $1-\gamma$, $\gamma = 1.8$ as we did for the 3C 295 ACF, and we found the correlation angle $\theta_0 = 1.2^{+1.3}_{-1.0}$ arcsec (90% confidence limit). This is lower that of 3C 295 by a factor of $\gtrsim 2$ at a confidence level of 2.5 σ.

4. Discussion

A 92 ks *Chandra* observation of the source field around the $z = 0.46$ 3C 295 cluster shows an excess of sources visible in the NE corner of the *Chandra* observation (fig. 1). This is clear in the density contour plot of fig. 11. This figure shows that the denser region of the putative filament has a sources density more than 5 times higher than the average source density of the field (~ 0.5 sources per arcmin^2. A chip by chip logN-logS analysis demonstrates that the NE chip has a 4.0σ excess of sources over the SW chip in the total ($0.5-7$ keV) *Chanda* band. [In the standard soft ($0.5-2$ keV) band the excess is 3.2σ, and in the standard hard ($2-7$ keV) band the excess is 3.3σ.] This result confirms the basic result of Cappi et al. (2001) and extends it to deeper fluxes, larger field-of-view and the $2-10$ keV band.

The asymmetric distribution of the 3C 295 field is confirmed by two analyses: (1) the two dimensional Kolmogorov-Smirnov test, which show the probability that the sources are uniformly distributed is 0.632% in the

Table 3. KS test for CDFS and 3C 295 fields

	3C 295[a]	CDFS[a]	CDFS[b]
$0.5-2$ keV	$3.09\ 10^{-2}$	0.2	0.13
$2-7$ keV	$3.84\ 10^{-2}$	0.5	0.17
$0.5-7$ keV	$6.32\ 10^{-3}$	-	-

[a] lux limits: $0.5-2$ keV, $F_X > 4.5\times10^{-16}$ ergs s^{-1} cm^{-2}; $2-7$ keV, $F_X > 3.5\times10^{-15}$ ergs s^{-1} cm^{-2}; $0.5-7$ keV, $F_X > 7.8\times10^{-16}$ ergs s^{-1} cm^{-2}.
[b] flux limits: $0.5-2$ keV, $F_X > 6.0\times10^{-17}$ ergs s^{-1} cm^{-2} $2-7$ keV, $F_X > 5.0\times10^{-16}$ ergs s^{-1} cm^{-2}.

Table 4. *Chandra* **fields chosen for the ACF analysis**

field	exposure time	number of sources		
	(ks)	$0.5-2$ keV	$2-7$ keV	$0.5-7$ keV
NGC55	60	108	75	132
WHDF	72	83	58	104
ISO	74	92	76	116
GROTH-WEST.F	85	84	63	103
1156+295	75	145	50	150
Elais:N1	74	101	80	127
Elais:N2	74	85	60	102
FIELD-142549+35	122	110	96	148

total *Chandra* band [3.09 % for the soft band and 3.84 % for the hard band). (2) the two point angular correlation function (ACF) strongly indicate positive correlation, for scales of $0.5-5$ arcmins. This strong correlation has not been found in a sample of eight ACIS-I fields with a similar exposure time, for which the correlation angle θ_0 is smaller by a factor of $\gtrsim 2$ than that of 3C 295 at the 2.5 σ confidence level, suggesting that the 3C 295 overdensity of sources in the NE chip is truly peculiar. An intriguing explanation, to be confirmed when the redshifts of the sources are measured, is that the overdensity of sources is actually related to a cosmic filament of the LSS.

Cappi et al. (2001) discussed four possible causes for this 'surplus' of sources: (1) gravitationally lensed very faint sources; (2) rapid evolution of cluster AGN or starburst galaxies; (3) cosmic variance of background sources; (4) LSS associated with the clusters. Since the surplus sources are not symmetrically place around the cluster, our results rule out an enhanced AGN population in the 3C 295 cluster itself, and lensing by the cluster potential. Since N-body and hydrodynamical simulations and galaxy surveys (e.g 2dF and Sloan) lead us to expect that clusters of galaxies lie at the nexus of several filament, we believe that this excess is likely to represent a filament of the LSS of the Universe converging onto the 3C 295 cluster.

The redshifts of the sources making up the excess are not yet known. However, if we assume that the sources are associated with the 3C 295 cluster, then we can use the cluster redshift to estimate some of their properties.

Adopting a concordance cosmology ($H_0 = 65$ km/s Mpc, $\Omega_M = 0.3$ and $\Omega_\Lambda = 0.7$, Spergel et al. 2003) we obtain luminosities in the range $7.5\times10^{41} \div 1.1\times10^{44}$ ergs s^{-1} (median $= 3.1\times10^{42}$ ergs s^{-1}) for the total *Chandra* band. [$2.8\times10^{41} \div 3.8\times10^{43}$ ergs s^{-1} (median $= 1.1\times10^{42}$ ergs s^{-1}) for the soft band; $1.5\times10^{42} \div 5.0\times10^{43}$ ergs s^{-1} (median $= 4.5\times10^{42}$ ergs s^{-1}) for the hard band.] These are moderate, Seyfert galaxy, luminosities, extending down to the range of luminous starburst galaxies at the faint end of the soft band.

An association with 3C 295 also defines a spatial scale of 2 Mpc (5 arcmin) for the adopted cosmology. For an, admittedly unlikely, spherical region of volume of ~ 4 Mpc^3 containing the excess sources, the implied space density of the excess sources (i.e. subtracting the CDF-S defined logN-logS contribution) is 0.9 Mpc^{-3} ($0.5-2$ keV) and 0.8 Mpc^{-3} ($2-10$ keV). This is well above the normal maximum AGN space density at $z = 0.5$ ($\sim 10^{-4}$ Mpc^{-3}, for luminosities down to 10^{42} ergs s^{-1} in the 0.5-2keV band, Hasinger 2003, and 10^{43} ergs s^{-1} in the 2-10 keV band Fiore et al. 2003). However, since the X-ray source luminosities are as low as $\sim 2\times10^{41}$ ergs s^{-1} (at the redshift of 3C 295), the little studied lower end of the XLF is being probed, and contributions from starburst and even normal galaxies can be important.

In fact, the integral of the field galaxy luminosity function at z=0.5 (e.g. Poli et al. 2001) gives ~ 0.13 galaxies Mpc^{-3} for $M_B < -17$ (a resonable faint end optical luminosity, corresponding to our lower X-ray luminosities). If we assume that roughly one tenth of the galaxies are active X-ray sources of $L_X > 3\times10^{41}$ ergs s^{-1}, then we would expect ~ 0.013 X-ray sources Mpc^{-3}. Since we count ~ 0.9 sources Mpc^{-3}, this implies a galaxy overdensity of ≈ 70, with of course a large (factor of 2-4) positive and negative uncertainty, because of the uncertainties in our space densities and assumptions. Still, this is intriguingly close to the expected galaxy overdensity of filaments $\sim 10 \div 10^2$, and much smaller than the overdensities of clusters of galaxies ($\sim 10^3 \div 10^4$), (the density contrast

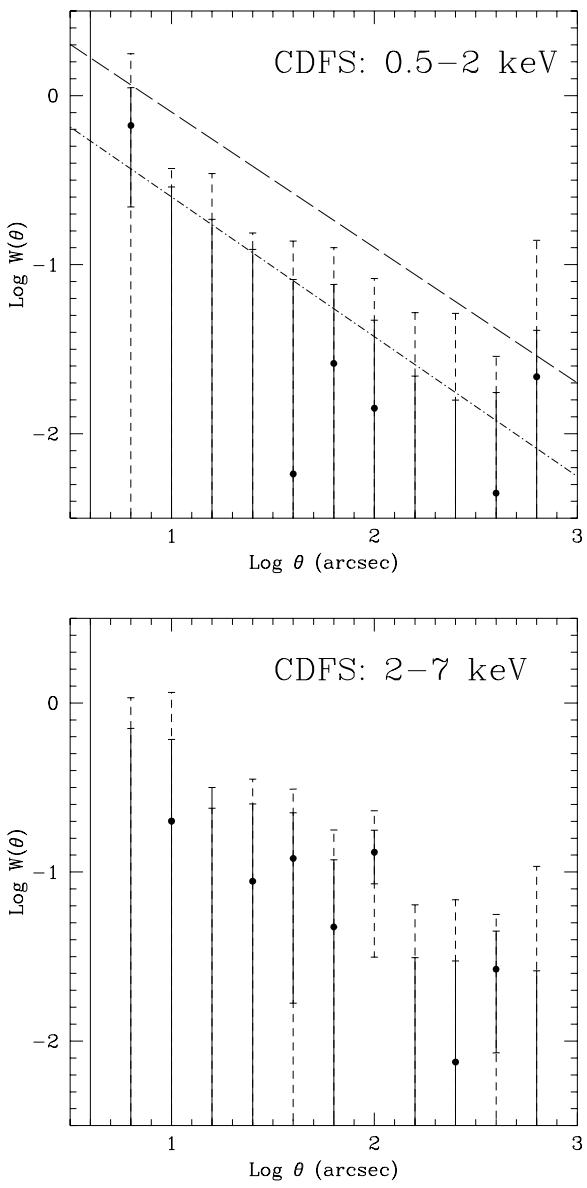

Fig. 9. The CDFS angular correlation function in the $0.5-2$ keV band (upper panel) and in the $2-7$ keV (lower panel). The dashed line line represents the best fit found by Vikhlinin & Forman (1995) for ROSAT sources; the dot-dashed line is the simulated ACF calculated by the same authors in order to correct the effect of the amplification bias. Solid error bars are Poisson; dashed error bars are bootstrap.

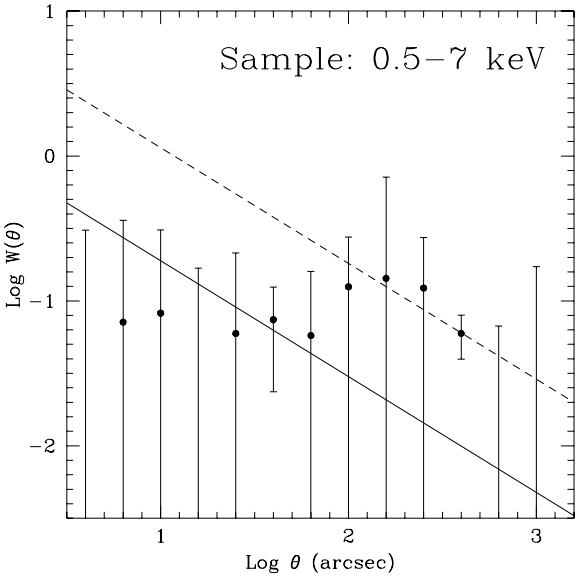

Fig. 10. The average angular correlation function in the $0.5-7$ keV band for the sample of fields reported in table 3; Error bars are bootstraps. The solid line represents the best fit for these data; the dashed line is the fit for the ACF of 3C 295 (see also fig. 8, bottom panel).

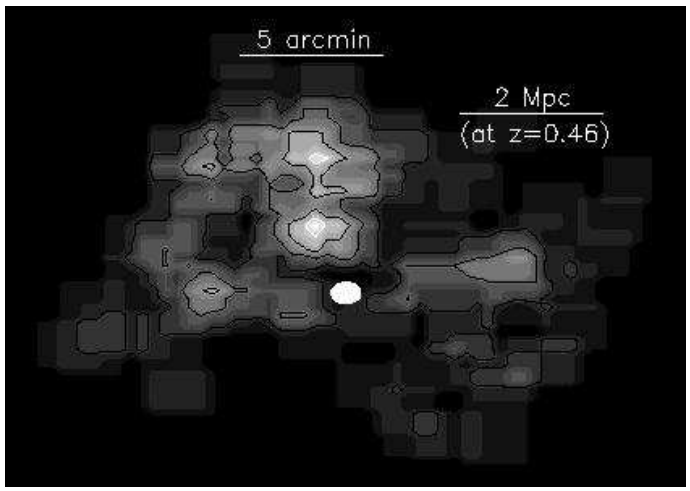

Fig. 11. The density profile of the 3C 295 field, computed for the whole $0.5-7$ keV band. The linear smoothing factor is 1.5 arcmin, and the four contour levels indicate source densities of 1.3, 1.8, 2.2 and 2.7 sources per arcmin^2. The clustering of sources in the NE corner is clearly visible; the bright central spot is the 3C 295 cluster.

at the virial radius being ~ 200). Furthermore, in a filamentary structure the implied space density will depend strongly on the orientation of the filament to our line of sight.

We stress again that these arguments hold only under the assumption that the redshift of the excess sources is the same of that of the 3C 295 cluster. In order to determine if this excess is associated or not to the 3C 295 cluster, we need to know the redshift of the sources via optical identifications.

For this reason, in order to study this candidate filament, we are pursuing new *Chandra* and optical observations to map out the 3C 295 region and delimiting the filament properties up to scales of ~ 24 arcmin (i.e. ~ 6 Mpc) from the 3C 295 cluster. These studies are important because they may open-up a new way to map high-density peaks of LSS at high redshifts with high efficiency.

Acknowledgements. We thank Dong-Woo Kim for careful reading of the manuscript and for useful comments. We are in debt with Salvo Sciortino, Giusi Micela and Francesco Damiani for providing us with the PWdetect algorithm and the relevant know how.

References

Almaini, O., Scott, S.E., Dunlop, J.S. et al. 2003, MNRAS, 338, 303
Barrow, J.D., Bhavsar, S.P. & Sonoda, D.H. 1984, MNRAS, 210, 19
Best, P.N., van Dokkum, P.G., Franx, M & Rottgering, H.J.A., 2002, MNRAS, 330, 17
Cappi, M., Mazzotta, P., Elvis, M. et al. 2001, ApJ, 548, 624
Daddi, E., Broadhurst, T., Zamorani, G., Cimatti, A., Roettinger, H., & Renzini, A., 2001, A&A 376, 825
Damiani, F., Maggio, A., Micela, G. & Sciortino, S., 1997a, ApJ, 483, 350
Damiani, F., Maggio, A., Micela, G. & Sciortino, S., 1997b, ApJ, 483, 370
Davé, R., Spergel, D.N., Steinhardt, P.J. & Wandelt, B.D., 2001, ApJ, 547, 574
Dickey, J.M. & Lockman, F.J., 1990, Ann. Rev. Ast. Astr.,ApJ...301..689H 28, 215.
Dressler, A. & Gunn, J.E., 1992, ApJS, 78, 1
Fasano, G. & Franceschini, A. 1987, MNRAS, 225, 155
Fiore et al. 2003, A&A, submitted
Fiore F., Nicastro, F., Savaglio, S., Stella, L. & Vietri, M., 2000, ApJL, 544, 7
Garmire, G.P., 1997, AAS, 29, 283
Giacconi, R., Zirm, A., Wang, J, et al. 2002, Apj, 139, 369
Giacconi, R., Rosati, P., Tozzi, P. et al. 2001, Apj, 551, 624
Giavalisco, M. & Dickinson, M., 2001, ApJ, 550, 177
Gilli, R., Cimatti, A., Daddi, E. et al. 2003, Accepted for pubblication in Apj (astro-ph/0304177)
Hasinger, 2003, astro-ph/0302574
Hasinger, G., Burg, R., Giacconi, R., Schmidt, M., Trumper, J. & Zamorani, g., 1998, A&A, 329, 482
Henry, J.P. & Henriksen, M.J., 1986, ApJ, 301, 689
Martini, P., Kelson, D.D., Mulchaey, J.S. & Trager, S.C., 2002, ApJL, 576 109
Mathur, S., Weinberg, D.H. & Chen, X. 2003, ApJ, 582, 82
Molnar, S.M., Hughes, J.P, Donahue, M. & Joy, M., 2002, ApJL, 573, 91
Nicastro, F., Zezas, A., Drake, J. et al., 2002, ApJ, 573, 157
Nicastro, F., Zezas, A., Elvis, M. et al., 2003, Nature, 421, 719
Peacock, J.A. 1983, MNRAS, 202, 615
Peacock, J.A. 1999, "Cosmological physics" (Cambridge: Cambridge University Press)
Peebles, P.J.E., 1980, " The Large Scale Structure of the Universe" (Princeton: Princeton University Press)
Pentericci, L., Kurk, J.D., Carilli, C.L., Harris, D.E., Miley, G.K. & Rottgering, H.J.A., 2002, astro-ph/0209392
Poli, F., Giallongo, E., Fontana, A., Cristiani, S. & D'Odorico, S., 2001, ApJL, 551, 45
Poli, F., Giallongo, E., Fontana, A., et al. 2003, ApJL, 593, 1
Rosati, P., Tozzi, P., Giacconi, R. et al., 2002, ApJ, 566, 667
Soltan, A.M., Freyberg, M.J. & Hasinger, G., 2002, A&A, 395, 475
Tozzi, P., Rosati, P., Nonino, M. et al., 2001, ApJ, 562, 42
Vikhlinin, A. & Forman, W., 1995, ApJL, 455, 109
Weisskopf, M.C.,, O'Dell, S.L. & Van Speybroeck, L.P., 1996, Proc. SPIE, 2805, 2
Yang, Y., Mushotzky, R.F., Barger, A.J., Cowie, L.L, Sanders, D.B., & Steffen, A.T., 2003, ApJL, 585, 85
Zappacosta, L., Mannucci, F, Maiolino, R. et al., 2002, A&A, 394, 7